Repetitive switching between DNA-binding modes enables target finding by the glucocorticoid receptor

Keizer, V.I.P.; Coppola, S.; Houtsmuller, A.B.; Geverts, B.; Royen, M.E. van; Schmidt, T.; Schaaf, M.J.M.

© 2019. Published by The Company of Biologists Ltd | Journal of Cell Science (2019) 132, jcs217455. doi:10.1242/jcs.217455

RESEARCH ARTICLE

Repetitive switching between DNA-binding modes enables target finding by the glucocorticoid receptor

Veer I. P. Keizer[1], Stefano Coppola[2], Adriaan B. Houtsmuller[3,4], Bart Geverts[3,4], Martin E. van Royen[3,4], Thomas Schmidt[2] and Marcel J. M. Schaaf[1,*]

ABSTRACT

Transcription factor mobility is a determining factor in the regulation of gene expression. Here, we have studied the intranuclear dynamics of the glucocorticoid receptor (GR) by using fluorescence recovery after photobleaching and single-molecule microscopy. First, we have described the dynamic states in which the GR occurs. Second, we have analyzed the transitions between these states by using a continuous-time Markov chain model and functionally investigated these states by making specific mutations in the DNA-binding domain. This analysis revealed that the GR diffuses freely through the nucleus and, once it leaves this free diffusion state, most often enters a repetitive switching mode. In this mode it alternates between slow diffusion as a result of brief nonspecific DNA-binding events, and a state of stable binding to specific DNA target sites. This repetitive switching mechanism results in a compact search strategy that facilitates finding of DNA target sites by the GR.

This article has an associated First Person interview with the first author of the paper.

KEY WORDS: Fluorescence recovery after photobleaching, Single-molecule microscopy, Glucocorticoid receptor, Transcription factor

INTRODUCTION

Transcription factors regulate gene expression by binding to specific DNA sequences and by recruiting other proteins. A well-studied transcription factor is the glucocorticoid receptor (GR), a member of the steroid receptor family, activated by glucocorticoid ligands. Upon ligand binding the receptor translocates to the nucleus where it interacts with DNA to initiate or repress transcription. By using biochemical assays, a wealth of knowledge has been obtained on the action of the GR at its DNA-binding sites. These DNA-binding sites, termed glucocorticoid response elements (GREs), are palindromic sequences that typically comprise two hexamers with a three-base pair spacer (Beato and Klug, 2000; Meijsing et al., 2009; Polman et al., 2013). The GR can also bind to other sequences, including negative GREs, albeit in a different conformation (Surjit et al., 2011; Hudson et al., 2013). Additionally, the GR can regulate gene expression by influencing the function of other transcription factors, either by binding to composite GREs or through a process called tethering (Ratman et al., 2013).

The development of live cell microscopy techniques using fluorescently tagged proteins enabled studies of the dynamic behavior of GR in the nucleus. The first investigations into the dynamics of the GR involved analysis by fluorescence recovery after photobleaching (FRAP) and, in more-recent years single-molecule microscopy (SMM) was used to further study the intranuclear dynamics of the GR. These studies revealed binding times in the order of seconds to the GREs (McNally et al., 2000; Schaaf and Cidlowski, 2003; Schaaf et al., 2005; Mueller et al., 2008). These transient immobilizations were found to be dependent on ligand activation and DNA binding of the GR, and are associated with transcriptional activity (Schaaf and Cidlowski, 2003; Stavreva et al., 2004; Schaaf et al., 2005; Morisaki et al., 2014). More-recent studies also revealed immobilizations at the sub-seconds scale (Groeneweg et al., 2014; Morisaki et al., 2014; Van Royen et al., 2014). Similar dynamic behavior has been uncovered for other steroid receptors (Stenoien et al., 2001; Farla et al., 2004, 2005; Marcelli et al., 2006; van Royen et al., 2007), as well as other transcription factors (Dundr et al., 2002; Gorski et al., 2008). In addition to these immobilizations, diffusive behavior through the nucleus has been observed for the GR (Gebhardt et al., 2013; Groeneweg et al., 2014; Morisaki et al., 2014; Paakinaho et al., 2017), and other bacterial and mammalian transcription factors, such as the lac repressor (Elf et al., 2007), STAT1 (Speil et al., 2011), p53 (Mazza et al., 2012; Morisaki et al., 2014), and the androgen receptor (AR) (Van Royen et al., 2014). For GR, and the transcription factors STAT1 and p53 (TP53), two diffusion states with distinct diffusion coefficients were found (Speil et al., 2011; Mazza et al., 2012; Gebhardt et al., 2013).

Together, these studies have demonstrated the occurrence of multiple dynamic states for transcription factors like the GR. However, the temporal relationship between these states is poorly understood because information on state-to-state transitions is not available. Furthermore, a consistent view that describes all states, including the biological processes underlying them, is still lacking. In our present study, we have combined FRAP and SMM experiments, which enabled a coherent analysis of GR dynamics over a time scale of milliseconds to seconds. We describe four dynamic states of the GR in detail. In addition, we have developed a continuous-time Markov chain (CTMC) model that provides information about the transitions between states of the GR as well as the time spent in each state. Finally, we have employed a series of mutations that influences the DNA-binding capacity to assess the biological processes underlying these states. Our results demonstrate that the GR spends most of its time in a repetitive switching mode, alternating between slow diffusion and immobile states. These periods of repetitive switching are interrupted by periods of fast diffusion. Our data provide a comprehensive description of the mechanism by which the GR finds its target sites.

[1]Animal Sciences and Health, Institute of Biology, Leiden University, 2333CC Leiden, The Netherlands. [2]Biological Matter/Living Systems, Institute of Physics, Leiden University, 2333CC Leiden, The Netherlands. [3]Department of Pathology, Erasmus Medical Center, 3000CA Rotterdam, The Netherlands. [4]Erasmus Optical Imaging Center, Erasmus Medical Center, 3000CA Rotterdam, The Netherlands.

*Author for correspondence (m.j.m.schaaf@biology.leidenuniv.nl)

T.S., 0000-0002-0045-1851; M.J.M.S., 0000-0002-5859-8936

Received 5 March 2018; Accepted 16 January 2019

Journal of Cell Science (2019) 132, jcs217455. doi:10.1242/jcs.217455

RESULTS

In all experiments described here, a well-characterized experimental system was used in which a YFP-GR fusion protein, comprising the human GR fused N-terminally to an enhanced yellow fluorescent protein (EYFP), was expressed in COS-1 cells (Fig. 1A) (Schaaf and Cidlowski, 2003; Schaaf et al., 2005; Groeneweg et al., 2014). In these studies it was demonstrated that the receptor mobility is dependent on the ligand, and in our present study the high-affinity synthetic glucocorticoid fluticasone propionate (FP) was used, which induces a maximal effect on the mobility of GR.

First, to study the mobility pattern of the GR in the nucleus of live cells, FRAP experiments were performed. For these measurements, photobleaching of YFP-GRs was performed by application of maximal laser power to a small strip spanning the nucleus. Subsequently, the recovery of the fluorescent signal was quantified over time (Fig. 1B) (van Royen et al., 2009). The experimental recovery curves were quantitatively analyzed using Monte Carlo simulations. Three states were detected: a diffusion state in which 55±2% of all molecules resided, a short immobile state (26±1%) and a long immobile state (19±2%). The short and long immobile states were characterized by short (0.7±0.1 s) and long (3.5±0.9 s) immobilization times, respectively. The results are summarized in Fig. 1C (the diffusion coefficient of the molecules in the diffusion state was obtained from the analysis of the SMM experiments (see below), and was used as a fixed parameter in the simulations).

To obtain a more complete overview of the mobility pattern of the GR, FRAP was complemented with SMM experiments. Where FRAP experiments give information on the seconds time scale, providing more details on the immobile states, SMM measures dynamics at the sub-second timescale, providing additional information on the diffusing fractions. Moreover, cross-validation was possible where the results of the two methods overlapped. Image sequences were taken with a time lag of 6.25 ms (Fig. 1D),

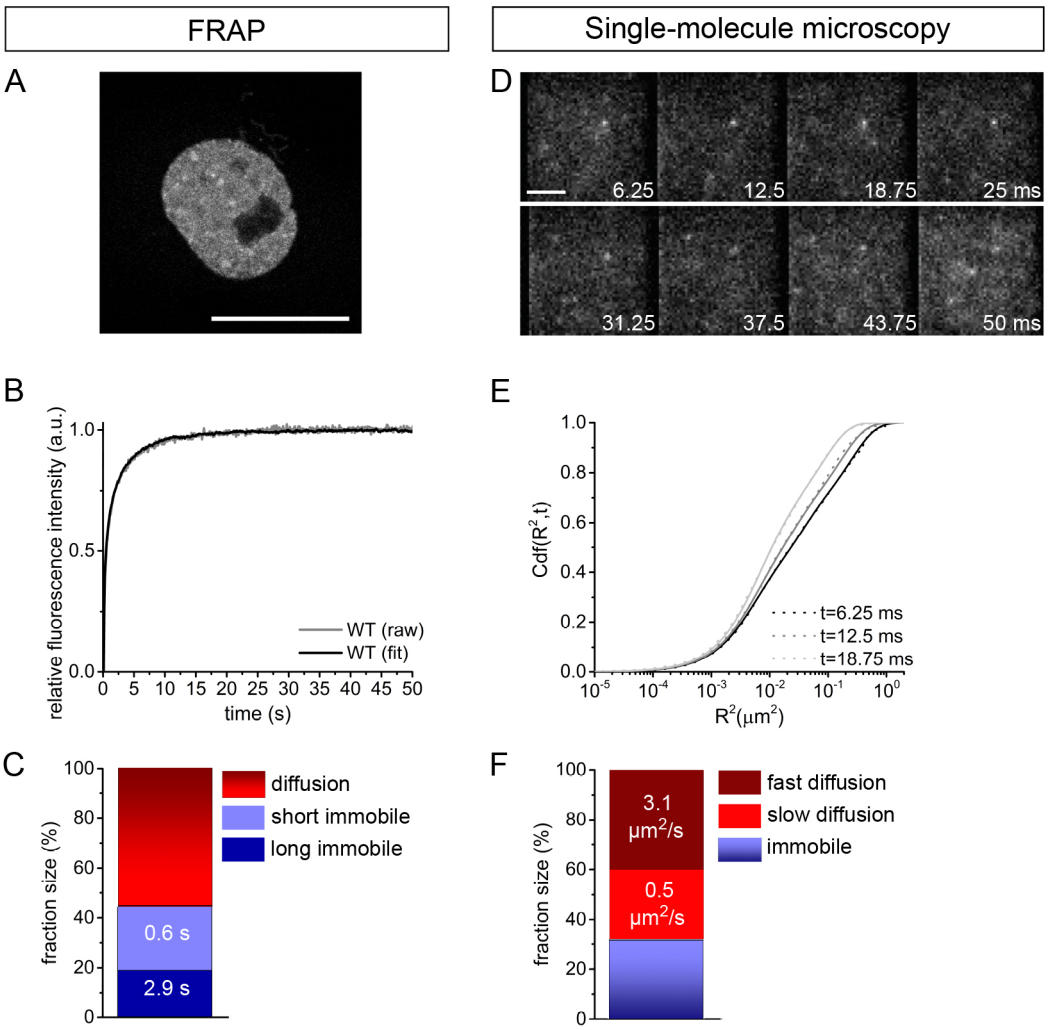

Fig. 1. Analysis of WT YFP-GR dynamics by using FRAP and SMM. (A) Representative confocal microscopy image of COS-1 cells expressing WT YFP-GR, 2 h post activation with ligand (FP, 5 nM); scale bar: 5 µm. (B) FRAP curve of WT YFP-GR. The bleach pulse was given at t=0 s. In each experiment, data points from >30 cells were pooled. The orange line represents the average of the top ten best fits. (C) WT YFP-GR distribution over the diffusion state, the short immobile state and the long immobile state. The time spent in either immobile state is indicated. Data shown are means from five independent experiments. (D) Sequence of eight single-molecule images of a COS-1 cell expressing WT YFP-GR. A signal-to-noise ratio of ∼16 was determined (see Fig. S1). Scale bar: 5 µm. (E) Cumulative distribution function of squared displacements for three time lags (6.25, 12.5 and 18.75 ms). Representative distributions shown are based on one independent experiment (more than seven cells, 15 sequences of eight frames were taken per cell, resulting in >4000 particle localizations per experiment). (F) WT YFP-GR distribution over the fast diffusion state, the slow diffusion state and the immobile state. The diffusion coefficients of the diffusion states are indicated. Data shown are means of five independent experiments.

Journal of Cell Science (2019) 132, jcs217455. doi:10.1242/jcs.217455

and the mobility of molecules was analyzed using particle image-correlation spectroscopy (Semrau and Schmidt, 2007). In this method, all possible correlations between the location of molecules in consecutive frames are determined. This way, a cumulative distribution function (*Cdf*) of displacements *R* is generated. This function was generated for the interval between subsequent frames, and between frames two or three lag times apart (resulting in 12.5 or 18.75 ms lag time, respectively).The *Cdf* for YFP-GR using these three different time lags is shown in Fig. 1E. The curves were fitted with a 3-population model, which fitted the results better than a 2-population model and was chosen for two reasons. First, analysis of the same data using a different (unbiased) approach based on phasors demonstrated that two diffusing fractions were present (S.C., V.I.P.K., M.J.M.S. and T.S., unpublished data). Second, in previous studies fitting the data with one diffusing fraction yielded a diffusing fraction for which the diffusion coefficient was dependent on the DNA-binding capacity of the receptor (see also Groeneweg et al., 2014). However, we assume that the fastest component of the mobility pattern of GR should be independent of its DNA-binding capacity. As will be presented below, when we used a model with two diffusing fractions, the fast diffusing fraction appeared to be independent of the DNA-binding capacity.

The results of the fitting showed that 40±7% of YFP-GR molecules occurred in a fast diffusion state, 28±4% in a slow diffusion state and 32±4% in an immobile state. The fast and slow diffusion states were characterized by a fast (3.1±0.4 $\mu m^2/s$) and slow (0.5±0.08 $\mu m^2/s$) diffusion constant, respectively. The results are summarized in Fig. 1F. In SMM it is not possible to distinguish the short and long immobilization events found in FRAP (which are in the order of seconds) due to the short time scale of the experiments (in the order of milliseconds).

To determine the average time the receptors reside in a given state and the probabilities of their transition to another state, we developed a CTMC model. In this model, random times spent in a state are exponentially distributed, and GRs were allowed to switch between three states (i.e. a fast diffusion, slow diffusion and an immobile state). Model parameters were extracted from fraction sizes and the diffusion coefficients that were found by using SMM and the combined immobilization times from FRAP (see Materials and Methods, Fig. S1). Owing to the ensemble nature of the data used as input for the model in this study, ranges were determined for all parameters. Within these ranges, the values of all parameters were uniformly distributed.

By using this approach, we found that YFP-GR spent more than 7.5 s in the fast diffusion state, whereas the average time spent in the slow diffusion state ranged between 1.2 and 1.4 s (Fig. 2A). Furthermore, the CTMC model revealed a high transition probability from the fast to the slow diffusion state (>0.80), but a low transition probability to the immobile state (<0.20) (Fig. 2B). From the slow diffusion state, the probability to switch to the immobile state was between 0.75 and 0.95, whereas the probability to transit to the fast diffusion state was between 0.05 and 0.25. From the immobile state, the probability of transition to the slow diffusion state was >0.95 and to the fast diffusion state <0.05. The transitions and time spent in each state have been summarized in Fig. 2C.

From this model emerges a likely transition path that is followed by the GR in order to reach its target site. The GR showed a remarkably strong preference for transitions from the fast to slow diffusion state, from the slow diffusion state to an immobile state and from an immobile state to the slow diffusion state. To further illustrate the implications of the results of the CTMC model, we employed numerical simulations. In these simulations, the behavior

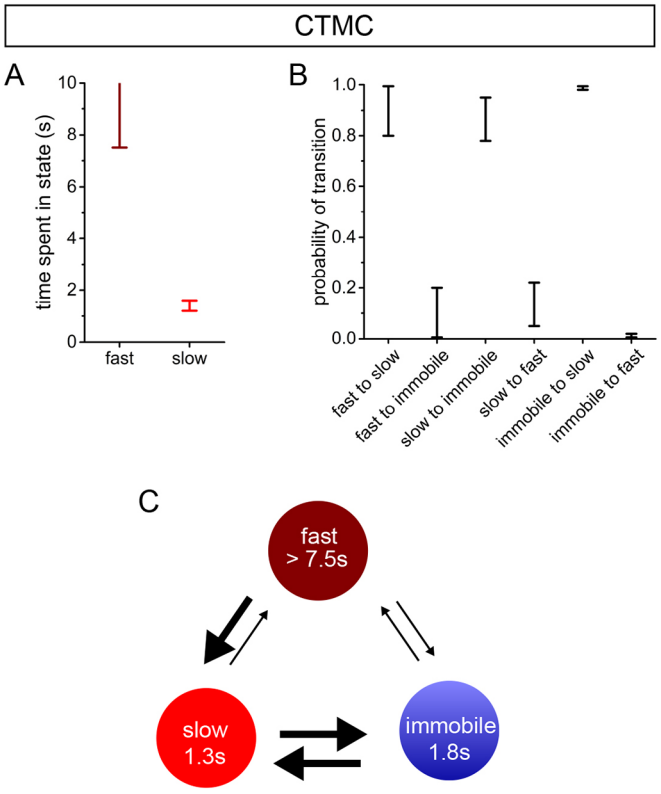

Fig. 2. The CTMC model applied to SMM data of WT YFP-GR. (A) Time spent in states for WT YFP-GR. The CTMC model used here provides value ranges that are likely to represent the true average time spent in this state. These ranges are indicated in the graph. The range for the time spent in the fast state only has a lower limit. (B) Probability of transitions between states for WT YFP-GR. Like in A, ranges of values are indicated. (C) Schematic overview of data presented in A and B, showing probabilities of transition between states (as shown in A; denoted by the arrows) and times spent in the state (as shown in B; reported in the circles).

of an individual molecule was described based on the times spent in the immobile, slow diffusion and fast diffusion states, and the transition probabilities between these states. A representative diagram showing the simulated behavior of a GR molecule over a period of 200 s is presented in Fig. 3A. These results reveal that individual receptors spent a long time in the fast diffusion state but, once it enters the slow diffusion state, it will switch repetitively between the slow diffusion and the immobile states before returning to the fast diffusion state. This is visualized by a spatial representation of a numerical simulation, in which the behavior of an individual molecule is described based on the times spent in the immobile, slow diffusion and fast diffusion states, and the transition probabilities between these states (Fig. 3B).

Next, we investigated the role of each of the states in GR function. We focused on assessing the DNA-binding properties of GR in each of the states by using six mutants of the human GR (hereafter referred to as K442A, V443A, R447K, R477K, C438Y and ΔDBD) (see Materials and Methods and Fig. 4A). Regarding the first four of these mutants, their site of mutation was selected on the basis of the crystal structure of the GR DNA-binding-domain (DBD) bound to a GRE (Luisi et al., 1991). Amino acids K442 and V443 had been predicted to share hydrogen bonds with nucleobases that are specific to the GRE sequence (Nordeen et al., 1990; Luisi et al., 1991). Mutation of K442 reduces the ability of the GR to initiate transcription (Meyer et al., 1997). A naturally occurring mutation

Journal of Cell Science (2019) 132, jcs217455. doi:10.1242/jcs.217455

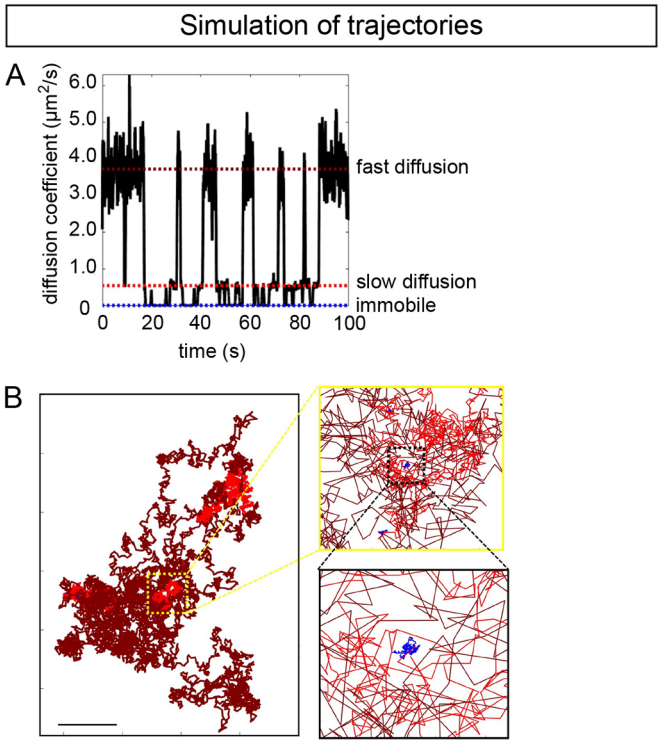

Fig. 3. Numerical simulation of the behavior of an individual molecule. The behavior was simulated based on the times spent in the different states and the transition probabilities between these states as shown in Fig. 2. (A) Diagram showing transitions between states over time, showing that the GR spends relatively long periods of time in the fast diffusion state and, once it has left this state, repetitively switches between the slow diffusion and immobile state, before returning to the fast diffusion state. (B) Trajectory of the GR moving through the cell nucleus (colors represent different states as described in Fig. 2; scale bar: 2 µm). This trajectory illustrates the compact searching strategy of the GR as a result of repetitive switching. Once the GR has left the free diffusion state (dark red), it slows down owing to nonspecific interactions (light red), keeping it in a restricted area, in which it binds to its specific target sites (blue).

of the equivalent amino acid V443 in the AR renders this receptor unable to initiate transcription and leads to complete androgen insensitivity in patients (Lobaccaro et al., 1996). Amino acid R447 had been predicted to interact with a GRE-specific nucleobase and with backbone components of the DNA (Luisi et al., 1991), whereas amino acid R477 was predicted to solely have interactions with the backbone of the DNA (Luisi et al., 1991). Mutation in AR of the equivalent amino acid of R447 renders the receptor unable to recognize cognate response elements (Shaffer et al., 2004) and has been shown to alter its intranuclear dynamics (Van Royen et al., 2014). Mutation of R477 renders the GR unable to initiate transcription and results in shorter recovery time in FRAP experiments (Kino et al., 2004). Moreover, this mutation naturally occurs in humans leading to primary cortisol resistance (Ruiz et al., 2001). Regarding the fifth mutant (C438Y), residue C438 was mutated to disrupt the structure of the DBD because it is one of the four cysteine residues creating the first zinc finger by non-covalently binding Zn^{2+}. The sixth mutant (ΔDBD) comprises the deletion of the entire DBD (amino acids 428–490) (Hollenberg et al., 1987). Representative confocal images of cells expressing each mutant receptor are presented in Fig. S2A.

The effect each mutation or deletion has on the *in vitro* DNA-binding capacity was determined using an ELISA-based DNA-binding assay. COS-1 cells were transfected with wild-type (WT) or mutant YFP-GR expression vectors. Nuclear extracts were prepared, and the relative capacity of binding to GREs was determined for serial dilutions of these extracts. Subsequently, DNA-binding capacity was plotted against the relative protein concentrations in the nuclear extract, determined by measuring YFP fluorescence. For WT and mutant YFP-GRs, a one-phase association equation was used to fit the data (Fig. S2B). Subsequently, the maximal DNA-binding capacity relative to WT YFP-GR was determined for each mutant (Fig. 4B). Mutation of K442 or V443 had no significant effect on relative maximal DNA-binding capacity of the GR. Mutation of amino acids R447 and R477 significantly reduced the relative maximal-binding capacity of the GR (52%±4% and 43% ±8%, respectively), as did mutation of C438 (54%±6%). The ΔDBD mutant showed lowest relative maximal binding of GR to GREs (17%±2%). Since we had not included a control lysate without overexpressed YFP-GR, this observed residual binding may be the result of nonspecific binding to other proteins in the lysate or of nonspecific DNA interactions of the ΔDBD mutant. Taken together these YFP-GRs (WT and mutants) show a range of different DNA-binding capacities, with WT YFP-GR having the highest and the YFP-GR ΔDBD mutant having the lowest.

We next considered the ability of each mutant to initiate transcription. To assess this, a reporter assay was performed in which luciferase gene expression was controlled by a MMTV promoter, containing multiple GREs. In this assay, all mutants showed significantly reduced luciferase activity compared to WT YFP-GR (Fig. 4C). The transactivation capacity (relative to WT) of mutants V443A and R447K was 28±2% and 32±14%, respectively, whereas the transcriptional activity of mutants K442A, C438Y, R477K and ΔDBD was comparable to background level (8±1%, 3±1%, 10±3% and 5±3%, respectively). The reduced ability of mutants R447K, R477K, C438Y and ΔDBD to initiate transcription corresponded with their reduced DNA-binding capacity. Interestingly, mutants K442A and V443A were found to be significantly reduced in their ability to activate gene transcription, although they showed only negligible reduction in DNA-binding capacity.

By using the DBD mutants, we studied the relationship between the mobility pattern of the GR and the DNA-binding capacity. For this purpose, we first performed FRAP experiments with all mutant YFP-GRs (FRAP curves and fits are shown in Fig. S3). The percentage of molecules in the diffusion state ranged from 55±2% for WT YFP-GR – which displayed the highest DNA-binding capacity, to 80±4% for the ΔDBD mutant – which had the lowest DNA-binding capacity of all mutants (Fig. 5). A correlation analysis showed that the fraction of YFP-GR molecules in the diffusion state negatively correlated with the DNA-binding capacity (Fig. S4A). The size of the fraction of YFP-GR molecules in the short immobile state was similar to that in WT and mutants (~20%) (Fig. 5B, Fig. S4B), indicating that occurrence of this state does not depend on DBD-mediated interactions inside the nucleus. However, slight differences regarding the time spent in this state were observed (ranging from ~0.5 to ~0.7 s; Fig. 5C), and these values correlated with those of the DNA-binding capacity (Fig. S4C). Finally, the fraction size of YFP-GR molecules in the long immobile state ranged from 19±2% (for WT YFP-GR) to 23±1% and 7±2% (for K442A and V443A, respectively), to the complete absence of this fraction (other mutants with a lower DNA-binding capacity) (Fig. 5D). This size positively correlated with the DNA-binding capacity (Fig. S4D), as did the immobilization time of this state (Fig. 5E, Fig. S4E). Moreover, reduction in DNA-binding capacity

Journal of Cell Science (2019) 132, jcs217455. doi:10.1242/jcs.217455

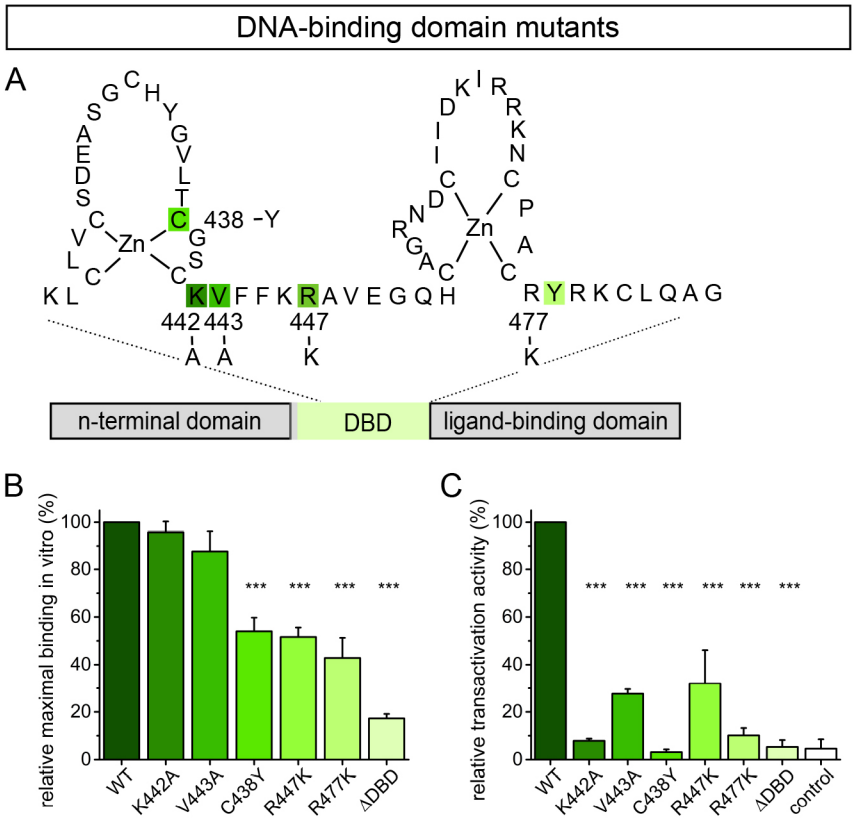

Fig. 4. Characterization of DNA-binding domain mutants of the human GR. (A) Schematic diagram of the GR comprising three domains, the N-terminal domain (aa 1–416), the DNA-binding domain (DBD, aa 417–490) and the ligand-binding domain (aa 491–770). The amino acid sequence for the DBD is given and the mutations used in the present study are indicated. (B) DNA-binding capacity of YFP-GR (WT or mutant) to a GRE *in vitro*. Nuclear extracts were taken from COS-1 cells expressing YFP-GR (WT or mutant) activated with ligand (FP, 5 nM). GR present in these extracts was allowed to bind to a GRE *in vitro* for 1 h. Subsequently, GR binding was measured using an ELISA-based approach. The maximal binding was determined (see Fig. S2), and the relative maximal binding is presented for WT and mutant YFP-GR (mean±s.e.m. of three independent experiments). (C) Transactivation activity of YFP-GR (WT or mutant) in luciferase reporter assay. MMTV-luciferase and CMV-Renilla reporter constructs and YFP-GR (WT or mutant) expression vectors were transfected into COS-1 cells and the luciferase activity was measured after FP (5 nM) administration. The relative activity of WT and mutant YFP-GR is shown (mean ±s.e.m. of three independent experiments). As a control, the procedure was performed without cells. ***P<0.01, statistically significant differences compared to WT control

resulted in complete loss of YFP-GR molecules in the long immobile state, suggesting that this state represents direct DBD-mediated DNA binding.

Subsequently, we studied the effect DNA-binding capacity has on the intranuclear dynamics by using SMM. First, a negative correlation between the size of fraction of YFP-GR molecules in the fast diffusion state and DNA-binding capacity was found (Fig. S5A), ranging from ∼40% (WT) to ∼61–64% (mutants ΔDBD, R477K, R447K and C438Y) (Fig. 6A). The diffusion coefficient of molecules in this fast diffusion state was not affected by mutations in the DBD (Fig. 6B, Fig. S5B). Second, both the fraction of YFP-GR molecules in the slow diffusion state and the diffusion coefficient of molecules in this state were independent of the DNA-binding capacity (Fig. 6C,D, Fig. S5C,D). Third, the size of the fraction of YFP-GR molecules in the immobile state was not influenced by mutation of K442 or V443, but mutants C438Y, R447K, R477K and ΔDBD showed a significant decrease compared to WT (respectively 17±4%, 14±6%, 10±3% and 11±3% compared to 32±4%, Fig. 6E). This fraction size positively correlated with the DNA-binding capacity (Fig. S5E).

Finally, the CTMC model was applied to analyze data acquired on the dynamics of the DBD mutants. No effect of the DNA-binding capacity was observed on the time spent in the fast diffusion state. All mutants had a lower limit for the time spent in this state comparable to WT YFP-GR (7.5 s) (Fig. 7A). In contrast, the average time spent in the slow diffusion state was affected by the DNA-binding capacity. With one exception (K442A), mutants spent less time on average in this state (0.4–0.9 s); mutant K442A spent a similar time in the slow diffusion state as WT YFP-GR (Fig. 7B). These results indicate that the time spent in the slow diffusion state is dependent on the DNA-binding capacity of the GR, whereas the time spent in the fast diffusion state is not. Like the WT YFP-GR, all mutant YFP-GRs showed a strong preference for transitions from fast to slow diffusion state, from slow to an immobile state and from an immobile to the slow diffusion state. None of the transitions between states was affected by the DNA-binding capacity (Fig. S6A–F).

DISCUSSION

In this study, we have identified the different states in which the GR occurs in the nucleus. This analysis was done on the basis of its dynamic behavior that was assessed by using FRAP and SMM. To determine the biological processes underlying these states, we used six mutants yielding reduced DNA-binding capacities. The DNA-binding capacity of these mutants appeared to correlate well with certain mobility parameters, even though this capacity was measured *in vitro*. Additionally, we have developed a CTMC model to determine the time spent in all states and the probability of state-to-state transitions. By combining the data obtained in these descriptive and functional studies, we obtained a comprehensive overview of GR dynamics, which is shown in Fig. 8. In this overview, all dynamic GR states are presented, as well the temporal relations between these states and their function. We present a mechanism on how the GR finds its target, in which repetitive switching between nonspecific and specific DNA binding modes plays a central role.

We used a combination of two techniques – FRAP and SMM – both of which have disadvantages and advantages (reviewed in Mueller et al., 2013). Nevertheless, by using both these techniques we were able to discriminate between diffusing and immobile states of GR. Although we still lack direct evidence, we assume that FRAP and SMM identify the same diffusing and immobile states because the substantial difference in kinetics between diffusing and immobile populations of molecules makes them easily distinguishable with both techniques. In addition, FRAP yields

Journal of Cell Science (2019) 132, jcs217455. doi:10.1242/jcs.217455

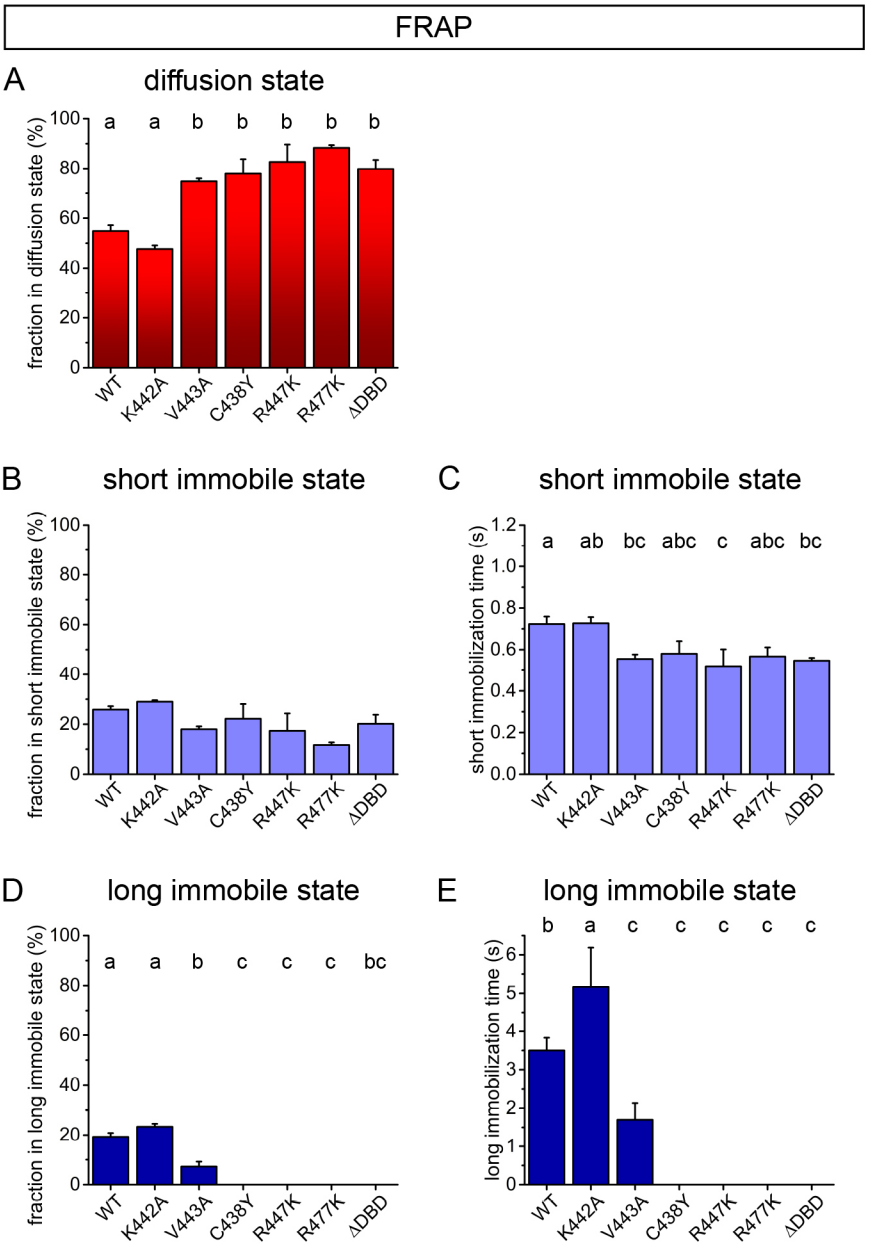

Fig. 5. FRAP analysis of WT and mutant YFP-GR dynamics. (A) Size of the fraction of YFP-GRs (WT or mutant) in the diffusion state. (B) Size of the fraction of YFP-GRs (WT or mutant) in the short immobile state. (C) Immobilization time of short immobile fraction of YFP-GRs (WT or mutant). (D) Size of the fraction of YFP-GRs (WT or mutant) in the long immobile state. (E) Immobilization time of long immobile fraction of YFP-GRs (WT or mutant). Data shown are average values ±s.e.m. of three independent experiments (for WT, five independent experiments were used). For each condition in each experiment >30 cells were used. Statistical significance between groups (P<0.01) is indicated by letters; groups with the same letters belong to a homogenous subset, i.e. are not significantly different.

better resolution over a longer period of time (seconds) and SMM over shorter periods (milliseconds). As a result, with FRAP we were able to 'split up' the immobile state, demonstrating the occurrence of a short and a long immobile state. By using SMM, we were able to distinguish between two diffusing states, and demonstrate the occurrence of a fast and a slow diffusing state. Thus, by combining FRAP and SMM data, we identified a total of four different states on the basis of their dynamic behavior.

The fast diffusion state was interpreted as representing freely diffusing GRs, since neither the diffusion coefficient nor the time spent in this state was dependent on the DNA-binding capacity of GR. The diffusion coefficient found for this state (3.1 $\mu m^2/s$) is within the same range as GR diffusion coefficients reported in other studies (9.2 $\mu m^2/s$; Gebhardt et al., 2013) and, especially, that of other transcription factors, including p53 and STAT1 (3.4 and 3.1 $\mu m^2/s$, respectively; Speil et al., 2011; Mazza et al., 2012). These freely diffusing GRs are likely to occur as dimers or in complex with other proteins (Hager et al., 2009; Presman et al., 2014).

The slow diffusion state was characterized by a sixfold lower diffusion coefficient than that of the fast diffusion state (0.5 $\mu m^2/s$). The time spent in this state was largely dependent on the DNA-binding capacity of the receptor, indicating that the diffusion rate of these molecules was affected by interactions with DNA. We suggest that these DNA interactions are nonspecific and include short sections of sliding, hopping and intersegmental exchange (van Royen et al., 2011; Hammar et al., 2012; Normanno et al., 2012; Izeddin et al., 2014). Nonspecific DNA interactions on a time scale of milliseconds have been observed previously in bacteria (Elf et al., 2007).

The short immobile state has previously been interpreted as nonspecific DNA binding by us and others (Chen et al., 2014; Groeneweg et al., 2014; Van Royen et al., 2014) but, in this present study, its occurrence appeared to be independent of a functional DBD. We, therefore, suggest that this state represents interactions with DNA that are mediated through the ligand-binding domain or the N-terminal domain. The short immobilization

Journal of Cell Science (2019) 132, jcs217455. doi:10.1242/jcs.217455

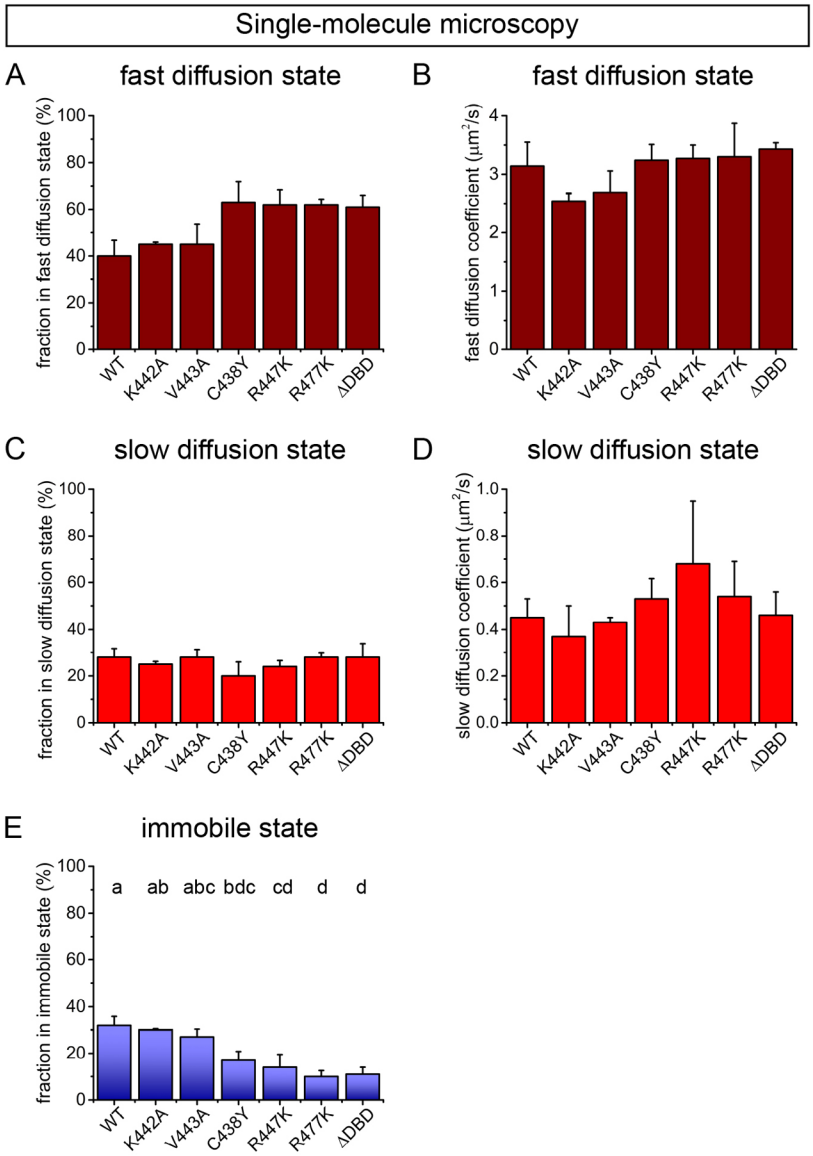

Fig. 6. SMM analysis of WT and mutant YFP-GR dynamics. (A) Size of the fraction of YFP-GRs (WT or mutant) in the fast diffusion state. (B) Diffusion coefficient of YFP-GR (WT or mutant) in the fast diffusion state. (C) Size of the fraction of YFP-GRs (WT or mutant) in the slow diffusion state. (D) Diffusion coefficient of YFP-GR (WT or mutant) in the slow diffusion state. (E) Size of the fraction of YFP-GRs (WT or mutant) in the immobile state. Data shown are average values ±s.e.m. of three independent experiments (for WT five independent experiments were used). For each condition in each experiment more than seven cells were used. Statistical significance between groups (P<0.01) is indicated by letters; groups with the same letters belong to a homogenous subset, i.e. are not significantly different.

events – which last ∼0.6 s – could represent tethering events for which direct DNA binding is not necessary and through which the GR is known to regulate the activity of other transcription factors (Kassel and Herrlich, 2007; Ratman et al., 2013). Indeed, it has recently been shown that, when AP-1 – a known tethering partner for the GR – is knocked out, the fraction of GRs occurring in the short immobile state is reduced (Paakinaho et al., 2017).

According to our data, the long immobile state depended entirely on the DNA-binding capacity of the receptor. We observed

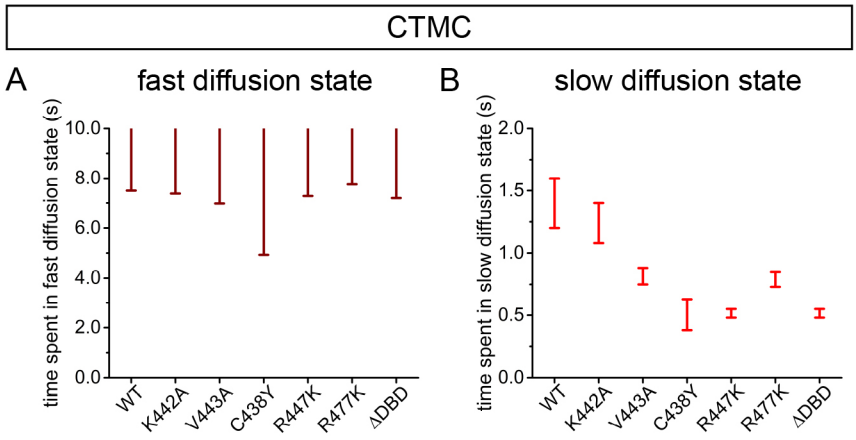

Fig. 7. Time spent in different diffusion states for YFP-GR (WT or mutant). The CTMC model, applied to the SMM data, provides ranges of values that are equally likely to represent the true average time spent in this state. These ranges are indicated in the graphs. (A) Time spent in fast diffusion state for YFP-GR (WT or mutant). In this case, the analysis provided only a lower limit for the time spent in the state. (B) Time spent in slow diffusion state for YFP-GR (WT or mutant).

Journal of Cell Science (2019) 132, jcs217455. doi:10.1242/jcs.217455

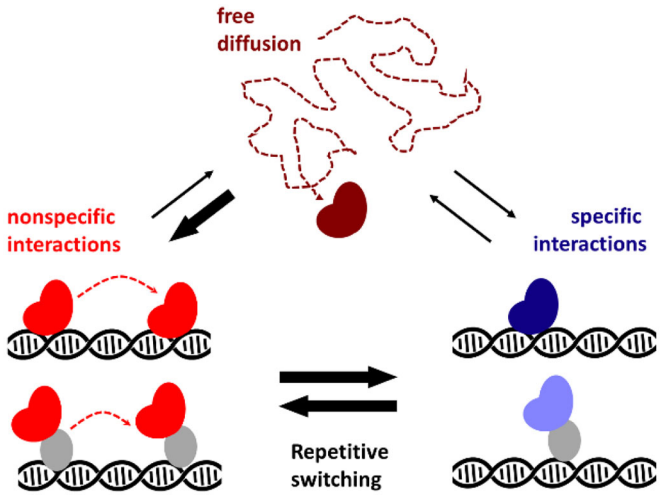

Fig. 8. Repetitive switching results in a compact searching strategy. Schematic overview of the intranuclear behavior of the GR, summarizing the results obtained in the present study. By combining data from FRAP and SMM, four different states were identified, which are represented by different colors: a fast diffusion state which is freely diffusing through the nucleus (brown), a slow diffusion state in which GRs interact nonspecifically with DNA (red), and a short and long immobile state in which receptors interact specifically with DNA, indirectly (light blue) and directly (dark blue), respectively. The occurrence of the two diffusion states was demonstrated by SMM, and the occurrence of the two immobile states by FRAP. The probability of transition between states is indicated by arrows. The thickness of the arrows represents the likeliness of the transition. After leaving the free diffusion state, GRs most often enter a repetitive switching mode, in which it alternates between specific and nonspecific interactions.

a total absence of molecules in this state when the DNA-binding capacity of the receptor was significantly compromised. This state was interpreted as representing direct specific DNA-binding by the GR. The long immobilization time of ∼2.9 s is similar to that observed for the GRs bound to GREs in live cells (McNally et al., 2000; Morisaki et al., 2014). In the latter study, this population is only present at transcriptionally active sites in the nucleus.

By using the CTMC model, we demonstrate a repetitive switching mechanism for the GR, in which the receptor repeatedly alternates between brief nonspecific DNA interactions and longer immobilizations due to specific DNA binding (Fig. 6A). Apparently, a period of specific DNA binding is most frequently preceded by a period of nonspecific DNA binding, which suggests that the nonspecific DNA-binding state facilitates localization of the specific DNA target sites. It has previously been proposed that these nonspecific DNA interactions are necessary to reach a specific site (van Royen et al., 2011; Hammar et al., 2012; Normanno et al., 2012; Chen et al., 2014; Izeddin et al., 2014). During the repetitive switching the GR remains in a restricted area. As a result, two subsequent specific binding events most often occur at sites that are in close proximity. Thus, repetitive switching is the mechanism through which the searching strategy of transcription factors is compacted. This is visualized by spatial representation of a numerical simulation, in which the behavior of an individual molecule was described on the basis of time spent in immobile, slow diffusion or fast diffusion states, and of the transition probabilities between these states (Fig. 3B). Compact search strategies have been proposed before, as a way to facilitate target finding (Hager et al., 2009; Izeddin et al., 2014) and, here, we present repetitive switching as the mechanism through which the GR compacts its target searching.

These periods of repetitive switching are preceded by extended periods of free diffusion through the nucleoplasm. Interestingly, the GR spends on average >10 s in the free diffusion state. With a diffusion coefficient of 3.1 $\mu m^2/s$, this allows it to traverse large areas of the nucleus unhindered. It is, therefore, highly unlikely that it does not encounter accessible DNA, which strongly suggests that the GR is unable to bind DNA in this state. This could be explained by the GR entering the repetitive switching mode through a conformational change or complex formation, which enables it to interact with DNA. This process may involve multimerization of the receptor (Presman et al., 2016).

The use of a variety of mutants provided a powerful tool to investigate the effect of the DNA-binding capacity on GR dynamics, but it also was relevant in order to establish which amino acid/base pair interactions are crucial in GR function. Changes in amino acids R447 and R477 completely abolished the long immobilization times, suggesting that R447 and R477 – which are known to interact with the backbone of the DNA – are of great importance to stabilize binding of DNA to GREs. This is in line with a previous study, describing that mutation of R477 results in increased mobility in FRAP experiments (Kino et al., 2004).

Mutation of amino acids K442 and V443 showed little effect on DNA binding *in vitro* or on the immobilization times of the receptor in living cells. However, these mutants are compromised in their ability to activate transcription, showing that DNA binding alone is not sufficient to initiate transcription. K442 and V443 are known to directly interact with GRE-specific nucleobases (Nordeen et al., 1990; Luisi et al., 1991). We, therefore, suggest that the interactions between K442 and V443, and specific nucleobases involve a conformational modification that is crucial to initiate transcription, alluding to an allosteric modulation of the GR by DNA to achieve additional specificity (Meijsing et al., 2009).

In summary, we have described and interpreted the dynamics of the GR, and present a detailed picture of the behavior of transcription factors in the nucleus. We reveal a mechanism by which a transcription factor reaches its cognate recognition sequence, which involves repetitive switching of the GR between a state of nonspecific and specific DNA binding.

MATERIALS AND METHODS

DNA constructs

Five individual point mutations were made in the pEYFP-GR plasmid (Schaaf and Cidlowski, 2003), yielding mutants C438Y, K442A, V443A, R447K and R477K. Mutagenesis was carried out using the QuikChange II Site-Directed Mutagenesis Kit (Agilent, Santa Clara, CA). Successful mutation was confirmed by sequence analysis. A sixth mutant, ΔDBD, lacking amino acids 428–490, i.e. the entire DBD, had been created earlier (described as Δ428–490 by Schaaf and Cidlowski, 2003). For luciferase assays, two additional plasmids were used: pMMTVluc, containing the mouse mammary tumor virus (MMTV) promoter adjacent to the firefly luciferase cDNA sequence, and pRL (Promega, Madison, WI) containing the cytomegalovirus (CMV) promoter adjacent to the Renilla luciferase cDNA.

Cell culture and transfection

COS-1 cells were originally obtained from American Type Culture Collection (ATCC, Manassas, VA). Monthly checks on mycoplasma and other bacterial infections were performed. Cells were cultured in Dulbecco's modified Eagle's medium (DMEM, ThermoFisher Scientific, Waltman, MA) without Phenol Red, supplemented with 10% fetal calf serum (FCS) at 37°C and 5% CO_2. One day prior to transfection, cells were plated in 6-well plates. When cells were used for imaging, coverslip glasses (ThermoFisher Scientific), were placed at the bottom of the well prior to plating the cells. Transfection was carried out using FuGENE HD (Promega, Madison, WI), according to the manufacturer's instructions. Briefly, for each well, a mix

was made containing 500 ng of DNA and 3 µl of FuGENE in a total volume of 500 µl DMEM. This mix was incubated at room temperature for one hour and added to the cells. Medium was refreshed the following day.

Confocal laser scanning microscopy

For confocal microscopy, cells were transfected with a pEYFP-GR plasmid encoding the wild-type receptor or a mutated version. One day post transfection fluticasone propionate (FP, 5 nM, Sigma-Aldrich, Zwijndrecht, The Netherlands) was added. Three to six hours after addition of the ligand, coverslips onto which the cells had been plated were placed in a metal ring holder and 1 ml of DMEM without FCS was added. Confocal images of the cells were taken using a Leica SPE confocal microscope equipped with a 488 nm laser and a 100×/1.4NA oil immersion objective (Leica Microsystems, Amsterdam, The Netherlands).

DNA-binding assay and luciferase reporter assay

Cells were transfected with the pEYFP-GR plasmid (WT or a mutated version). One day post transfection FP (5 nM) was added. Three hours after addition of the ligand, nuclear extracts were collected using the Nuclear Extraction kit (Active Motif, La Hulpe, Belgium). More than 5×10^6 cells were used per sample. In order to measure the relative YFP-GR concentrations in the samples, fluorescence intensities of the lysates were determined using a Turner BioSystems Modulus microplate reader (Promega, Madison, WI). A series of eight 1:2 dilutions of these samples was used to perform a DNA-binding assay using the GR TransAM kit (Active Motif, La Hulpe, Belgium) following the manufacturer's instructions. The sequence of the oligonucleotide used to measure the GR binding was 5′-GGTACAnnnTGTTCT-3′. DNA-binding activity was assessed by measuring absorbance at 450 nm wavelength, corrected for background illumination at 600 nm using the Turner BioSystems Modulus microplate reader (Promega, Madison, WI). A negative control measurement (without cellular extract) was used to correct the obtained values at both wavelengths. The determined DNA-binding activities were plotted as a function of the relative fluorescence intensities of the lysates, combining data points from the three independent experiments. A one-phase association equation was used to fit the data:

$$y = y_o + (B_{max} - y_0)(1 - e^{-ks}), \quad (1)$$

where y_0 is the y-intercept and B_{max} is the plateau value. The determined value for k was then used as a constant on the curve of each individual experiment to more accurately determine B_{max}, which represents the maximal binding achieved at the YFP-GR concentration range used in this experiment (Graphpad Software, La Jolla, CA). This maximal binding was normalized to the maximal binding of the WT YFP-GR. The data shown are averages (±s.e.m.) of the three independent experiments. A one-way ANOVA was performed by using a Holm-Sidak test to correct for multiple comparisons (OriginLab, Northampton, MA). Statistical significance was accepted at $P<0.01$.

For the luciferase assay, cells were transfected with pEYFP-GR plasmid (WT or a mutated version), the MMTV plasmid and the CMV plasmid simultaneously. Transfected cells were induced with FP (5 nM) for up to 10 h. Adherent cells were lysed using passive lysis buffer (Promega, Madison, WI). More than 1×10^6 cells were used per sample. The dual-luciferase reporter assay system was used to detect firefly and Renilla luciferase activities (Promega, Madison, WI). Luciferase activity was measured using the Turner BioSystems Modulus Microplate reader (Promega, Madison, WI). As a control, the procedure was performed without cells. The data shown are averages (±s.e.m.) of the three independent experiments. A one-way ANOVA was performed with a Bonferroni test to correct for multiple comparisons (OriginLab, Northampton, MA). Statistical significance was accepted at $P<0.01$.

Fluorescence recovery after photobleaching

Cells were transfected with the plasmid pEYFP-GR (WT or a mutated version). One day after transfection and 3–6 h prior to imaging, FP (5 nM) was administered. The coverslip on which the cells were grown was placed into a metal ring holder and 1 ml of DMEM without FCS was added. Cells were imaged at 37°C for a maximum of 2 h using a Zeiss LSM510 META confocal laser scanning microscope with a 40×/1.3NA oil-immersion objective (Carl Zeiss, Breda, The Netherlands). Fluorescence recovery after photobleaching (FRAP) experiments were performed as described previously (Groeneweg et al., 2014; Van Royen et al., 2014). Briefly, a narrow strip spanning the entire width of the nucleus was scanned at 514 nm excitation [using an argon laser (30 mW)] with short intervals (100 ms) at low laser power. Fluorescence intensity was recorded using a 560-nm long pass filter. After 40 frames a high intensity (100% laser power) 100 ms bleach pulse was administered and recovery of fluorescence at the bleached strip was monitored for 55 s at 100 ms intervals. Fluorescence intensities were normalized to baseline intensity and FRAP curves were generated by plotting the fluorescence intensity over time. For each receptor (WT or mutant), at least 30 cells were imaged per experiment and three independent experiments were performed.

To analyze the experimental FRAP curves quantitatively, they were compared to curves generated using Monte Carlo simulations. This method has been described extensively (van Royen et al., 2009; Geverts et al., 2015) and was used to determine the mobility pattern of AR and GR (Groeneweg et al., 2014; Van Royen et al., 2014). The used software is available upon request. A 3-population model was used, containing a diffusing population and two populations characterized by distinct immobilization times. A model with two immobile populations fits the data significantly better than a model with one immobile population. Under certain conditions, however, only one immobile population was found, indicating the absence of a bias (Van Royen et al., 2014). The computer-simulated curves were subsequently compared to the experimental data by least squares analysis. For this purpose, the diffusion coefficient of the mobile subpopulation obtained from the analysis of the SMM experiments was used as a fixed parameter. This left four parameters as variables: the sizes of the short immobile and the long immobile population (both in the range of 0–90%), and the times spent in the short and long immobile state (0.1–1 s and 1–300 s, respectively).

The data shown are averages (±s.e.m.) of the three independent experiments. Data were statistically analyzed using the restricted maximum likelihood (REML) approach with a linear mixed model using Genstat (VSNi, Hemel Hempstead, UK). The fixed part of the model consisted of factors (measurement) day and cell line (control and mutants), while the random part contained block (day) and cells within block. Residuals were checked for the equal variance assumption. Comparisons of means/homogenous subsets were based on Fischer's protected least significance difference test. In addition, values for each parameter were plotted as a function of the relative maximal DNA-binding capacity. Regression analysis was performed by ANOVA (OriginLab, Northampton, MA). Statistical significance was accepted at $P<0.01$.

Single-molecule microscopy

One day after transfection with the pEYFP-GR plasmid (WT or a mutated version), FP (5 nM) was administered to the cells. Between 3 and 6 h after FP administration, coverslips containing the transfected cells were placed into a metal ring holder and 1 ml DMEM was added. Cells were imaged at 37°C and 5% CO_2 for a maximum of 2 h using a wide-field fluorescence microscope equipped with a 100×/1.4NA oil-immersion objective (Carl Zeiss, Breda, The Netherlands) as described previously (Groeneweg et al., 2014; Van Royen et al., 2014; Harkes et al., 2015). Illumination was performed using a 514 nm argon laser at an intensity of 4 kW/cm^2. Illumination of the sample for 3 ms was controlled through an acousto-optical tunable filter (AA Opto Electronic, Orsay, France). Cells expressing the fluorescent proteins were photobleached until individual fluorescence signals could be distinguished. Images were recorded on a back-illuminated CCD camera (Princeton, Instruments, Trenton, NJ) before being digitized (0.202 µm/pixel). Three individual experiments were performed. Cells were randomly selected. In each experiment, seven cells were imaged for each mutant. For each cell, fifteen sequences of eight frames were taken. The time lag between subsequent frames was 6.25 ms.

The location of individual molecules was determined by fitting a 2D Gaussian to each signal [all custom scripts used for the analysis of single-molecule microscopy (SMM) data are available upon request (Schmidt

et al., 1996; Harms et al., 2001)]. The location of the molecule was defined by the center of this peak determined to an accuracy of 0.16 pixels (32 nm). Individual peaks were excluded based on a threshold for the relative localization error. Subsequently, the mobility was analyzed by combining data from all sequences of eight frames (for each experimental condition, more than 4000 molecule localizations were recorded per individual experiment). Analysis was performed using particle image-correlation spectroscopy (PICS; Semrau and Schmidt, 2007), using up to three successive intervals between frames. In PICS analysis, individual particles are not tracked, but all possible correlations between the location of molecules in consecutive frames are determined. This way, a cumulative distribution function (*Cdf*) of displacements R is generated. This function was generated for the interval between subsequent frames, and between frames two or three lag times apart (resulting in 12.5 ms and 18.75 ms lag time, respectively). For each time interval, a 3-population model was used to fit the data, in order to determine the fraction of molecules α in each of the three populations and their respective diffusion coefficients (D). The model is given by the following equation:

$$Cdf\,(R^2) = 1 - \left[\alpha_1 \exp\left(\frac{R^2}{4D_1 t + 4\sigma^2}\right) - \alpha_2 \exp\left(\frac{R^2}{4D_2 t + 4\sigma^2}\right) - \alpha_3 \exp\left(\frac{R^2}{4\sigma^2}\right)\right]. \quad (2)$$

The data shown are averages (±s.e.m.) of the three independent experiments. Data were statistically analyzed by restricted maximum likelihood (REML) with a linear mixed model using Genstat (VSNi). The fixed part of the model consisted of factors (measurement) day and cell line (control and mutants), while the random part contained block (day) and cells within block. Residuals were checked for the equal variance assumption. Comparisons of means/homogenous-subsets were based on Fisher's protected least significance difference test. In addition, values for each parameter were plotted as a function of the relative maximal DNA-binding capacity. Regression analysis was performed by ANOVA (OriginLab, Northampton, MA). Statistical significance was accepted at $P<0.01$.

Continuous-time Markov chain model analysis

The cumulative probability distribution function (*Cdf*) obtained from the single-molecule data, was used to extract additional dynamic parameters and time scales of motions. Under the framework of a continuous-time Markov chain (CTMC) model, the exact occupation probability distribution was implemented for particles undergoing a three-state intermittent behavior between two diffusion states and one immobile state, as derived from (Coppola et al., 2014).

In brief, the cumulative distribution function $Cdf(R^2)$ has the following form:

$$Cdf\,(R^2) = R\int_0^\infty dk \boldsymbol{J}_1(k\boldsymbol{R}) e^{-\sigma^2 k^2} \mathcal{L}^{-1}[\boldsymbol{P}(k,s)], \quad (3)$$

where $\boldsymbol{J}(k\boldsymbol{R})$ is the Bessel function of the first kind (of order 1), σ is the positional accuracy, $\mathcal{L}^{-1}[\boldsymbol{P}(k,s)]$ is the inverse Laplace transform of the Fourier-Laplace occupation probability $\boldsymbol{P}(k, s)$. The three-state occupation probability $\boldsymbol{P}(k, s)$ used in the CTMC model is given by:

$$\boldsymbol{P}(k,s) = \frac{1}{2}\sum_{\substack{i=1\\ j=1}}^{3} [1 - \varphi_i(k,s)\varphi_j(k,s)]^{-1} \left[(1-\delta_{ij})\,\varphi_i(k,s)\varphi_j(k,s)\frac{\pi_j}{\lambda_i} + \delta_{ij}\varphi_i(k,s)\frac{\pi_i}{\lambda_j}\right], \quad (4)$$

where λ_i represents the average transition rate $\lambda_i=1/T_i$ (where T_i is the average time spent in the state i), $\varphi(k,s)=\lambda_i/(s+k^2D_i+\lambda_i)$ the mobility density of state i (with D_i as the diffusion coefficient), and π_i the steady-state probability. In the CTMC framework, these steady-state probabilities are defined from the relation:

$$\pi_1\ \pi_2\ \pi_3 \begin{pmatrix} -\lambda_1 & \lambda_1 p_{12} & \lambda_1 p_{13} \\ \lambda_2 p_{21} & -\lambda_2 & \lambda_2 p_{23} \\ \lambda_3 p_{31} & \lambda_3 p_{32} & -\lambda_3 \end{pmatrix} = \begin{pmatrix} 0 \\ 0 \\ 0 \end{pmatrix}, \quad (5)$$

where p_{ij} is the transition probability from state i to state j ($j\neq i$), under the conditions $0<p_{ij}<1$ and $\sum_{j=1,\,j\neq i}^{3} p_{ij} = 1\ \forall\ i = 1,\ 2,\ 3$. Hence, the steady-state probabilities are dependent on both the transition rates and the transition probabilities [i.e. $\pi_i \equiv \pi_i(\lambda_i, p_{ij})$ under the condition $\pi_1+\pi_2+\pi_3=1$]. In the model it is assumed that after spending the time T in one state, the molecule, must switch to either of the two remaining states. Hence, the probability of transition from the fast diffusion state to an immobile state was obtained as the complementary to 1 of the probability to transition from the fast diffusion state to the slow diffusion state. In the following, the immobile state was labeled as state '3', while the two diffusion states were labeled as '1' and '2'.

It is noteworthy to mention here that the three-state CTMC model introduces three additional free parameters to be estimated (i.e. the transition rates λ_1, λ_2, λ_3), with respect to the 3-population model for independent populations presented above. In addition, the non-linear dependency of the steady-state probabilities on the transition probability and rates highly affects the convergence of any fitting routine to an optimal solution. Indeed, a local minimum might give estimates of π_i and λ_i that inserted in the CTMC framework produce unacceptable values for the transition probabilities (i.e. $p_{ij}<0$ or $p_{ij}>1$). Therefore, for a robust estimation of the dynamic parameters, we decided to proceed with a multi-step optimization algorithm. First, we noted that for time scales smaller than the switching times, the three-state CTMC model can be well approximated by the three (independent) populations model. This condition was, indeed, held in our experiments in which the maximum time-lag (18.75 ms) was smaller than, for example, the immobilization times (~1 s) obtained from the FRAP analysis.

We then determined the dynamic parameters by fitting the *Cdf* with the three independent populations model (Fig. 1F). After fixing the average time spent in the immobile state $T_3=1/\lambda_3$, from Fig. S1B, we estimated the values for T_1 and T_2 that inserted in CTMC framework with $\pi_i\approx\alpha_i$ gave acceptable results for the transition probabilities (i.e. $0<p_{ij}<1$) (Fig. S1C). For every combination of T_1 and T_2 from the acceptable solutions (the time-steps can be arbitrarily small), we numerically calculated the theoretical *Cdf* for the CTMC model and the squared residuals, with respect to the estimated three independent populations model for the first time-lag t=6.25 ms. All values of the squared residuals below a given threshold corresponded to equally optimal values for T_1 and T_2. This threshold was defined as the residual value $Res(\hat{\imath})$ for which $(Res(\hat{\imath}) - \min(Res))/(\max(Res) - \min(Res)) = 5\%$. Therefore, it allowed us to set lower (and potentially upper) bounds for T_1 and T_2. For any optimal T_1–T_2 combination, we could additionally estimate the lower and upper bounds of the transition probabilities from CTMC framework (red solid line, Fig. S1D). Although we were seeking for three unknowns from three equations, the non-linearity of CTMC framework prevented us to obtain a single unique solution for every (π_1, π_2, π_3, T_1, T_2, T_3) combination. These limitations arise from the ensemble nature of our *Cdf*-based approach (i.e. $\pi_1+\pi_2+\pi_3=1$ holds without giving us access to the normalization factor that is necessary to uniquely solve the equation for the steady state probabilities).

Acknowledgements

The authors would like to thank Derk te Winkel for technical assistance and Paul Keizer (Wageningen University & Research) for help with the statistical analysis of the data.

Competing interests

The authors declare no competing or financial interests.

Author contributions

Conceptualization: V.I.P.K., A.B.H., M.E.v.R., T.S., M.J.M.S.; Methodology: V.I.P.K., S.C., A.B.H., M.E.v.R., T.S., M.J.M.S.; Software: V.I.P.K., S.C., A.B.H., B.G., M.E.v.R., T.S.; Validation V.I.P.K., S.C., B.G., M.E.v.R., M.J.M.S.; Formal analysis: V.I.P.K., S.C., B.G., M.E.v.R.; Investigation: V.I.P.K., S.C., B.G., M.E.v.R.; Resources: A.B.H., M.E.v.R., T.S.; Writing - original draft: V.I.P.K., M.J.M.S.; Writing - review & editing: V.I.P.K., S.C., A.B.H., M.E.v.R., T.S., M.J.M.S.;

Visualization: V.I.P.K., M.J.M.S.; Supervision: A.B.H., M.E.v.R., T.S., M.J.M.S.; Project administration: M.J.M.S.; Funding acquisition: M.J.M.S.

Funding
This work is part of the research programme of the Foundation for Fundamental Research on Matter (FOM), which is part of the Netherlands Organisation for Scientific Research (NWO).

Supplementary information
Supplementary information available online at
http://jcs.biologists.org/lookup/doi/10.1242/jcs.217455.supplemental

References

Beato, M. and Klug, J. (2000). Steroid hormone receptors: an update. *Hum. Reprod. Update* **6**, 225-236.
Chen, J., Zhang, Z., Li, L., Chen, B.-C., Revyakin, A., Hajj, B., Legant, W., Dahan, M., Lionnet, T., Betzig, E. et al. (2014). Single-molecule dynamics of enhanceosome assembly in embryonic stem cells. *Cell* **156**, 1274-1285.
Coppola, S., Caracciolo, G. and Schmidt, T. (2014). Exact occupation probabilities for intermittent transport and application to image correlation spectroscopy. *New J. Phys.* **16**, 113057.
Dundr, M., Hoffmann-Rohrer, U., Hu, Q., Grummt, I., Rothblum, L. I., Phair, R. D. and Misteli, T. (2002). A kinetic framework for a mammalian RNA polymerase in vivo. *Science* **298**, 1623-1626.
Elf, J., Li, G.-W. and Xie, X. S. (2007). Probing transcription factor dynamics at the single-molecule level in a living cell. *Science* **316**, 1191-1194.
Farla, P., Hersmus, R., Geverts, B., Mari, P. O., Nigg, A. L., Dubbink, H. J., Trapman, J. and Houtsmuller, A. B. (2004). The androgen receptor ligand-binding domain stabilizes DNA binding in living cells. *J. Struct. Biol.* **147**, 50-61.
Farla, P., Hersmus, R., Trapman, J. and Houtsmuller, A. B. (2005). Antiandrogens prevent stable DNA-binding of the androgen receptor. *J. Cell Sci.* **118**, 4187-4198.
Gebhardt, J. C. M., Suter, D. M., Roy, R., Zhao, Z. W., Chapman, A. R., Basu, S., Maniatis, T. and Xie, X. S. (2013). Single-molecule imaging of transcription factor binding to DNA in live mammalian cells. *Nat. Methods* **10**, 421-426.
Geverts, B., Van Royen, M. E. and Houtsmuller, A. B. (2015). Analysis of biomolecular dynamics by FRAP and computer simulation. *Methods Mol. Biol.* **1251**, 109-133.
Gorski, S. A., Snyder, S. K., John, S., Grummt, I. and Misteli, T. (2008). Modulation of RNA polymerase assembly dynamics in transcriptional regulation. *Mol. Cell* **30**, 486-497.
Groeneweg, F. L., Van Royen, M. E., Fenz, S., Keizer, V. I. P., Geverts, B., Prins, J., De Kloet, E. R., Houtsmuller, A. B., Schmidt, T. S. and Schaaf, M. J. M. (2014). Quantitation of glucocorticoid receptor DNA-binding dynamics by single-molecule microscopy and FRAP. *PLoS ONE* **9**, e90532.
Hager, G. L., Mcnally, J. G. and Misteli, T. (2009). Transcription dynamics. *Mol. Cell* **35**, 741-753.
Hammar, P., Leroy, P., Mahmutovic, A., Marklund, E. G., Berg, O. G. and Elf, J. (2012). The lac repressor displays facilitated diffusion in living cells. *Science* **336**, 1595-1598.
Harkes, R., Keizer, V. I. P., Schaaf, M. J. M. and Schmidt, T. (2015). Depth-of-focus correction in single-molecule data allows analysis of 3D diffusion of the glucocorticoid receptor in the nucleus. *PLoS ONE* **10**, e0141080.
Harms, G. S., Cognet, L., Lommerse, P. H. M., Blab, G. A. and Schmidt, T. (2001). Autofluorescent proteins in single-molecule research: applications to live cell imaging microscopy. *Biophys. J.* **80**, 2396-2408.
Hollenberg, S. M., Giguere, V., Segui, P. and Evans, R. M. (1987). Colocalization of DNA-binding and transcriptional activation functions in the human glucocorticoid receptor. *Cell* **49**, 39-46.
Hudson, W. H., Youn, C. and Ortlund, E. A. (2013). The structural basis of direct glucocorticoid-mediated transrepression. *Nat. Struct. Mol. Biol.* **20**, 53-58.
Izeddin, I., Récamier, V., Bosanac, L., Cissé, I. I., Boudarene, L., Dugast-Darzacq, C., Proux, F., Bénichou, O., Voituriez, R., Bensaude, O. et al. (2014). Single-molecule tracking in live cells reveals distinct target-search strategies of transcription factors in the nucleus. *eLife* **3**, e02230.
Kassel, O. and Herrlich, P. (2007). Crosstalk between the glucocorticoid receptor and other transcription factors: molecular aspects. *Mol. Cell. Endocrinol.* **275**, 13-29.
Kino, T., Liou, S. H., Charmandari, E. and Chrousos, G. P. (2004). Glucocorticoid receptor mutants demonstrate increased motility inside the nucleus of living cells: time of fluorescence recovery after photobleaching (FRAP) is an integrated measure of receptor function. *Mol. Med.* **10**, 80-88.
Lobaccaro, J. M., Poujol, N., Chiche, L., Lumbroso, S., Brown, T. R. and Sultan, C. (1996). Molecular modeling and in vitro investigations of the human androgen receptor DNA-binding domain: application for the study of two mutations. *Mol. Cell. Endocrinol.* **116**, 137-147.
Luisi, B. F., Xu, W. X., Otwinowski, Z., Freedman, L. P., Yamamoto, K. R. and Sigler, P. B. (1991). Crystallographic analysis of the interaction of the glucocorticoid receptor with DNA. *Nature* **352**, 497-505.
Marcelli, M., Stenoien, D. L., Szafran, A. T., Simeoni, S., Agoulnik, I. U., Weigel, N. L., Moran, T., Mikic, I., Price, J. H. and Mancini, M. A. (2006). Quantifying effects of ligands on androgen receptor nuclear translocation, intranuclear dynamics, and solubility. *J. Cell Biochem.* **98**, 770-788.
Mazza, D., Abernathy, A., Golob, N., Morisaki, T. and Mcnally, J. G. (2012). A benchmark for chromatin binding measurements in live cells. *Nucleic Acids Res.* **40**, e119.
Mcnally, J. G., Müller, W. G., Walker, D., Wolford, R. and Hager, G. L. (2000). The glucocorticoid receptor: rapid exchange with regulatory sites in living cells. *Science,* **287**, 1262-1265.
Meijsing, S. H., Pufall, M. A., So, A. Y., Bates, D. L., Chen, L. and Yamamoto, K. R. (2009). DNA binding site sequence directs glucocorticoid receptor structure and activity. *Science* **324**, 407-410.
Meyer, T., Starr, D. B. and Carlstedt-Duke, J. (1997). The rat glucocorticoid receptor mutant K461A differentiates between two different mechanisms of transrepression. *J. Biol. Chem.* **272**, 21090-21095.
Morisaki, T., Müller, W. G., Golob, N., Mazza, D. and McNally, J. G. (2014). Single-molecule analysis of transcription factor binding at transcription sites in live cells. *Nat. Commun.* **5**, 4456.
Mueller, F., Wach, P. and Mcnally, J. G. (2008). Evidence for a common mode of transcription factor interaction with chromatin as revealed by improved quantitative fluorescence recovery after photobleaching. *Biophys. J.* **94**, 3323-3339.
Mueller, F., Stasevich, T. J., Mazza, D. and Mcnally, J. G. (2013). Quantifying transcription factor kinetics: at work or at play? *Crit. Rev. Biochem. Mol. Biol.* **48**, 492-514.
Nordeen, S. K., Suh, B. J., Kühnel, B. and Hutchison, C. A. (1990). Structural determinants of a glucocorticoid receptor recognition element. *Mol. Endocrinol.* **4**, 1866-1873.
Normanno, D., Dahan, M. and Darzacq, X. (2012). Intra-nuclear mobility and target search mechanisms of transcription factors: a single-molecule perspective on gene expression. *Biochim. Biophys. Acta Gene Regul. Mech.* **1819**, 482-493.
Paakinaho, V., Presman, D. M., Ball, D. A., Johnson, T. A., Schiltz, R. L., Levitt, P., Mazza, D., Morisaki, T., Karpova, T. S. and Hager, G. L. (2017). Single-molecule analysis of steroid receptor and cofactor action in living cells. *Nat. Commun.* **8**, 15896.
Polman, J. A. E., De Kloet, E. R. and Datson, N. A. (2013). Two populations of glucocorticoid receptor-binding sites in the male rat hippocampal genome. *Endocrinology* **154**, 1832-1844.
Presman, D. M., Ogara, M. F., Stortz, M., Alvarez, L. D., Pooley, J. R., Schiltz, R. L., Grøntved, L., Johnson, T. A., Mittelstadt, P. R., Ashwell, J. D. et al. (2014). Live cell imaging unveils multiple domain requirements for in vivo dimerization of the glucocorticoid receptor. *PLoS Biol.* **12**, e1001813.
Presman, D. M., Ganguly, S., Schiltz, R. L., Johnson, T. A., Karpova, T. S. and Hager, G. L. (2016). DNA binding triggers tetramerization of the glucocorticoid receptor in live cells. *Proc. Natl. Acad. Sci. USA* **113**, 8236-8241.
Ratman, D., Vanden Berghe, W., Dejager, L., Libert, C., Tavernier, J., Beck, I. M. and De Bosscher, K. (2013). How glucocorticoid receptors modulate the activity of other transcription factors: a scope beyond tethering. *Mol. Cell. Endocrinol.* **380**, 41-54.
Ruiz, M., Lind, U., Gafvels, M., Eggertsen, G., Carlstedt-Duke, J., Nilsson, L., Holtmann, M., Stierna, P., Wikstrom, A.-C. and Werner, S. (2001). Characterization of two novel mutations in the glucocorticoid receptor gene in patients with primary cortisol resistance. *Clin. Endocrinol.* **55**, 363-371.
Schaaf, M. J. M. and Cidlowski, J. A. (2003). Molecular determinants of glucocorticoid receptor mobility in living cells: the importance of ligand affinity. *Mol. Cell. Biol.* **23**, 1922-1934.
Schaaf, M. J. M., Lewis-Tuffin, L. J. and Cidlowski, J. A. (2005). Ligand-selective targeting of the glucocorticoid receptor to nuclear subdomains is associated with decreased receptor mobility. *Mol. Endocrinol.* **19**, 1501-1515.
Schmidt, T., Schutz, G. J., Baumgartner, W., Gruber, H. J. and Schindler, H. (1996). Imaging of single molecule diffusion. *Proc. Natl. Acad. Sci. USA* **93**, 2926-2929.
Semrau, S. and Schmidt, T. (2007). Particle image correlation spectroscopy (PICS): retrieving nanometer-scale correlations from high-density single-molecule position data. *Biophys. J.* **92**, 613-621.
Shaffer, P. L., Jivan, A., Dollins, D. E., Claessens, F. and Gewirth, D. T. (2004). Structural basis of androgen receptor binding to selective androgen response elements. *Proc. Natl. Acad. Sci. USA* **101**, 4758-4763.
Speil, J., Baumgart, E., Siebrasse, J.-P., Veith, R., Vinkemeier, U. and Kubitscheck, U. (2011). Activated STAT1 transcription factors conduct distinct saltatory movements in the cell nucleus. *Biophys. J.* **101**, 2592-2600.
Stavreva, D. A., Muller, W. G., Hager, G. L., Smith, C. L. and Mcnally, J. G. (2004). Rapid glucocorticoid receptor exchange at a promoter is coupled to transcription and regulated by chaperones and proteasomes. *Mol. Cell Biol.* **24**, 2682-2697.

Journal of Cell Science (2019) 132, jcs217455. doi:10.1242/jcs.217455

Stenoien, D. L., Patel, K., Mancini, M. G., Dutertre, M., Smith, C. L., O'malley, B. W. and Mancini, M. A. (2001). FRAP reveals that mobility of oestrogen receptor-alpha is ligand- and proteasome-dependent. *Nat. Cell Biol.* **3**, 15-23.

Surjit, M., Ganti, K. P., Mukherji, A., Ye, T., Hua, G., Metzger, D., Li, M. and Chambon, P. (2011). Widespread negative response elements mediate direct repression by agonist-liganded glucocorticoid receptor. *Cell* **145**, 224-241.

Van Royen, M. E., Cunha, S. M., Brink, M. C., Mattern, K. A., Nigg, A. L., Dubbink, H. J., Verschure, P. J., Trapman, J. and Houtsmuller, A. B. (2007). Compartmentalization of androgen receptor protein-protein interactions in living cells. *J. Cell Biol.* **177**, 63-72.

Van Royen, M. E., Farla, P., Mattern, K. A., Geverts, B., Trapman, J. and Houtsmuller, A. B. (2009). Fluorescence recovery after photobleaching (FRAP) to study nuclear protein dynamics in living cells. *Methods Mol. Biol.* **464**, 363-385.

Van Royen, M. E., Zotter, A., Ibrahim, S. M., Geverts, B. and Houtsmuller, A. B. (2011). Nuclear proteins: finding and binding target sites in chromatin. *Chromosome Res.* **19**, 83-98.

Van Royen, M. E., van Cappellen, W. A., Geverts, B., Schmidt, T., Houtsmuller, A. B. and Schaaf, M. J. M. (2014). Androgen receptor complexes probe DNA for recognition sequences by short random interactions. *J. Cell Sci.* **127**, 1406-1416.